Control Engineering Practice 121 (2022) 105071

Contents lists available at ScienceDirect

Control Engineering Practice

journal homepage: www.elsevier.com/locate/conengprac

Iterative learning and feedback control for the curvature and contact force of a metal strip on a roll

G. Stadler [a,*], A. Steinboeck [b], L. Marko [a], A. Deutschmann-Olek [b], A. Kugi [a]

[a] Christian Doppler Laboratory for Model-Based Process Control in the Steel Industry, Automation and Control Institute, TU Wien, Gußhausstraße 27-29/376, 1040 Vienna, Austria

[b] Automation and Control Institute, TU Wien, Gußhausstraße 27-29/376, 1040 Vienna, Austria

ARTICLE INFO

Keywords:
Mechanical system
Mathematical models
Model inversion
Iterative learning control
Model based disturbance observer
Measurement results
Steel industry

ABSTRACT

This paper presents a novel model-based control strategy for the curvature and the contact force at the contact point of a metal strip and a roll. Due to the plastic deformation of the strip, the bending history of the strip has to be considered in the controller design. A multivariable two-degrees-of-freedom (2-DOF) control structure is used to track user-defined periodic references for the outputs. The proposed multi-input/multi-output (MIMO) feedback control structure consists of a spatial iterative learning control (ILC) combined with a multivariable PI controller. The control strategy is implemented in a real-time system and verified by measurements on an experimental test rig.

1. Introduction

1.1. Problem description and motivation

In strip processing plants, cold-rolled steel strips are heat treated in horizontal or vertical continuous annealing lines, Niederer et al. (2016) and Strommer et al. (2014). This heat treatment process controls material properties like strength, hardness, and ductility of the steel, Matthews and James (2010). A temperature range of 730 °C up to 1200 °C is characteristic for such annealing lines, see, e.g., Lankford (1985). The transport of the strip through a horizontal annealing line leads to a periodic strip-roll contact. This contact is also periodic for surface points of the rolls and can thus result in surface defects on the rolls, Fukubayashi (1995) and Sawa and Oohori (1995). Essentially, such surface defects are caused by mechanical and thermochemical effects, (cf. Moir & Preston, 2002; Munther & Lenard, 1999; Nioi et al., 2017). In case of severe roll surface defects, the strip quality may be impaired to an extent that the strip may even have to be scrapped. It is reported in Basabe and Szpunar (2004) and Min et al. (2012) that an increase in the furnace temperature also increases the frequency and size of the surface defects. In Nioi et al. (2019), a finite-element model was proposed to evaluate the evolution of surface defects. Statistical analysis of the factors that influence the surface defects are investigated in Jin et al. (2004). Automated inspection techniques incorporating process knowledge for the detection of surface defects are reported in Agarwal et al. (2011). A further example of such surface defects detection techniques is the combination of domain adaptation and adaptive convolutional neural networks presented in Zhang et al. (2021).

Another case of a periodic strip-roll contact is the bending leveler process. The primary objective of this process is a reduction of residual stresses and shape defects (residual curvatures) of the strip by alternate plastic bending of the strip between the rollers of the leveler. In fact, a bending leveler can generate a certain curvature in the strip. Using an analytical model of the consecutive bending process, force and power requirements of the leveling process are derived in Batty and Lawson (1965). However, the evolution of the curvature is neglected in Batty and Lawson (1965). In Kaiser et al. (2014), a desired residual stress state and the necessary sequence and amount of curvature are determined by simulations. In roller leveling, the elimination of a coil set of the strip does not guarantee that the desired residual stress distribution is achieved. Therefore, a combined approach of considering both the curvature and the residual stresses is proposed in Grüber et al. (2020). Many of the existing mathematical models in the literature are not suitable for real-time applications. Hence, a tailored real-time mathematical model for plate leveling is developed in Brauneis et al. (2018).

In summary, the development of surface defects is greatly influenced by process parameters, such as the steel grade of the strip, its temperature, the atmosphere, the strip curvature at the strip-roll contact point and the contact force between the strip and the roll. In order to study the mechanical conditions at the strip-roll contact point, the experimental test rig shown in Fig. 1 was built to test and

* Corresponding author.
E-mail address: stadler@acin.tuwien.ac.at (G. Stadler).

https://doi.org/10.1016/j.conengprac.2022.105071
Received 30 June 2021; Received in revised form 13 November 2021; Accepted 4 January 2022
Available online 25 January 2022

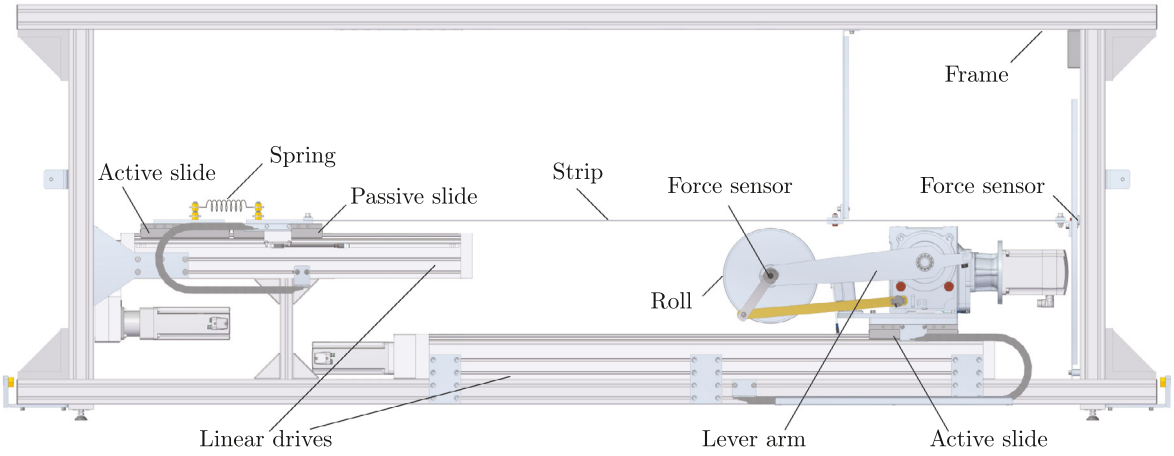

Fig. 1. Experimental test rig.

implement a control concept. In this paper, a model-based controller for the contact force q_{cp} and the strip curvature κ_{cp} at the strip-roll contact point x_{cp} is developed.

1.2. Experimental device and control problem

Fig. 2 shows a sketch and a snapshot during an experiment of the experimental device considered in this paper. This test rig closely resembles a simulation device at our industrial research partner voestalpine Stahl GmbH, Linz, Austria. The geometric dimensions of the test rig as well as the box constraints of the control inputs are almost equal in both devices. The test rig consists of a roll with radius R, whose horizontal position x_r and penetration depth z_r can be freely adjusted. Here, the penetration depth z_r equals the vertical distance between the upper vertex of the roll and the horizontal line through the mounting points of the strip. Furthermore, the position z_r represents a control input of the system, whereas the position x_r is an externally defined input which describes the periodic movement of the roll between the boundaries with a constant velocity v. The steel strip is fixed at the right boundary and attached to a passive slide at the left boundary, see Fig. 1. This passive slide is connected to an active slide by a spring. Another control input is the tensional force n in the strip, which is controlled by the relative displacement of the two slides. The contact force q_{cp} at the strip-roll contact point x_{cp} is measured by a force sensor located in the roll axle. For the estimation of the curvature κ of the strip, an infrared camera array was used, which will be described in Section 4.1. The length of the (plain) undeformed strip is denoted by L, its thickness by h, and the transverse deflection by w. The curvature κ_{cp} and contact force q_{cp} at the strip-roll contact point are system outputs that have to be controlled.

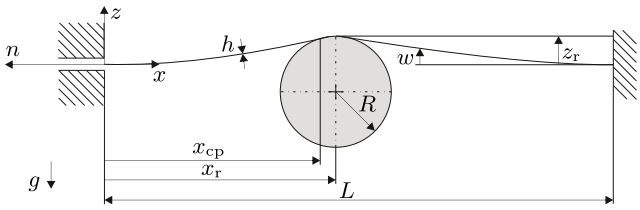

(a) Geometry of the experimental device.

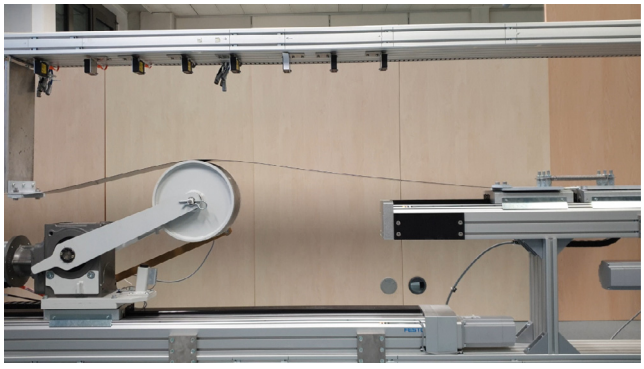

(b) Snapshot during an experiment.

Fig. 2. Geometry and snapshot of the experimental test rig.

1.3. Related work and contributions of this paper

Similar contact situations occur between the strip and looper rolls in tandem rolling mills, where the contact force between the strip and the looper roll is feedback controlled to ensure a certain strip tension, (cf. Choi et al., 2007; Steinboeck et al., 2014). In case of a periodic horizontal roll movement x_r, it is a reasonable assumption that the curvature κ of the strip will also undergo a periodic trajectory, at least in the steady state. Thus, the application of repetitive and iterative learning control techniques seems natural for controlling κ_{cp} and q_{cp}. These control techniques have been successfully applied in many fields of applications. Apart from industrial robotics, see, e.g., Gopinath and Kar (2004), Owens et al. (2013) and Wang et al. (2016), repetitive control approaches are used to prevent unknown periodic load disturbances for the eccentricity compensation in rolling, Garimella and Srinivasan (1994), as well as for the continuous steel casting process, Manayathara et al. (1996). Periodic tension fluctuations in reversing mills are suppressed in Asano et al. (2007) by a repetitive control approach. In Marko et al. (2020), the tracking of harmonic reference trajectories for a spindle drive in the presence of actuator backlash and sticking friction is achieved by a repetitive control scheme. A combination of an iterative learning controller (ILC) and a disturbance observer is presented in Maeda et al. (2015). The suggested control structure can reject near-repetitive disturbances and was successfully applied to an automated excavator in field trials. A Frequency-domain ILC for the control of a marine vibrator in order to suppress undesired frequencies is presented in Sörnmo et al. (2016). ILC is also used for the generation of ultrasonic wave pulses for nondestructive testing purposes, (cf. Upadhyay & Schaal, 2020), and for the control of ventricular assist devices with variable cycle durations, Ketelhut et al. (2019).

For the control task considered in this paper, a systematic consideration of the bending history of the strip is necessary because of a possible plastic deformation in the strip. The research presented in Stadler et al.

(2017), where a linear-elastic material model is considered, was verified in simulation studies only and is extended in the current paper. To the best of the authors' knowledge, a multi-input/multi-output (MIMO) control concept that considers the bending history of the strip does not exist in the literature. Therefore, the design of a multivariable two-degrees-of-freedom (2-DOF) control structure comprising a feedforward and a feedback part is proposed in this paper. The feedback part consists of a multivariable PI controller and a spatial ILC. This 2-DOF control structure has several advantages:

- By means of the feedforward control input, a reasonable control performance at the operating point is already achieved, which is further improved by the feedback controller.
- Spatially periodic disturbances and model-plant mismatches can be considered and eliminated by the ILC.
- The ILC feedback controller is independent of the horizontal velocity v_r of the roll, since spatial ILC means that the control law is parameterized with respect to the spatial position x_r instead of the usually chosen time t.
- Spatially acausal filters can be used to filter the control inputs in order to suppress measurement noise, which could otherwise lead to actuator vibrations.
- Remaining non-recurring disturbances are suppressed by the PI controller.

1.4. Structure of the paper

This paper is structured as follows: A material model, which considers the bending history of the strip, and a quasi-static strip deformation model are derived in Section 2. Section 3 outlines the design of a multivariable 2-DOF control structure comprising a feedforward and a feedback part, which is a combination of an ILC and a PI controller. Finally, measurement results from the laboratory experiment in Section 4 validate the proposed control strategy.

2. Mathematical model of the experimental rig

Throughout this paper, derivatives with respect to the spatial coordinate x are denoted by $(\cdot)' = \mathrm{d}(\cdot)/\mathrm{d}x$. The underlying assumptions of the material model presented in Section 2.1 and the quasi-static strip deformation model developed in Section 2.2 are given in full detail in Stadler et al. (2017). For the sake of completeness, only the most relevant parts are briefly summarized in the following. Due to the fact that a quasi-static model is considered, the time t is not included in Section 2 for the benefit of a compact notation.

2.1. Constitutive law of strip bending

An initially flat strip with zero residual stresses is assumed. In the following, a linear elastic/plastic constitutive law, which also considers the bending history, is derived. For this purpose, it is assumed that once a material point is plastically deformed, a plastic deformation in opposite direction does not occur (for the validity of this assumption in the considered system, see Section 3.1). Note that this assumption does not limit the applicability of the control law presented in Section 3. The control concept proposed in this paper can also be employed for more complex material laws. Let $m_\mathrm{b}(x)$ denote the bending moment of the strip normalized with respect to the strip width b, k_b the normalized bending stiffness, and $\kappa_0(x)$ the residual curvature of a strip cross section characterized by the coordinate x. Fig. 3 illustrates a typical bending history cycle of a material point. The curve is only plotted for positive values $m_\mathrm{b}(x)$ due to its point symmetry with respect to the origin. Furthermore, the curvature of the strip is defined by

$$\kappa(x) = \frac{w''(x)}{\left(1 + (w'(x))^2\right)^{\frac{3}{2}}}. \tag{1}$$

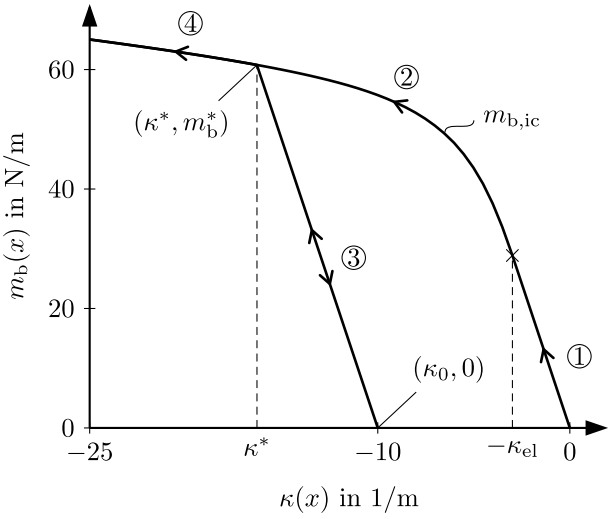

Fig. 3. Typical strip cross section bending history.

Starting with an initially plain strip, i.e. $\kappa(x) = \kappa_0(x) = 0$, the elastic part ① of the initial curve is traversed for $|\kappa(x)| \le \kappa_\mathrm{el}$. At the maximum elastic curvature κ_el, the outer fiber of the strip plastically deforms for the first time. Consequently, the initial curve $m_{\mathrm{b,ic}}(x)$ of the constitutive law between curvature and bending moment is given by

$$m_{\mathrm{b,ic}}(x) = \begin{cases} -k_\mathrm{b}\kappa(x) & \text{if } |\kappa(x)| \le \kappa_\mathrm{el} \\ f(\kappa(x)) & \text{if } |\kappa(x)| > \kappa_\mathrm{el} \end{cases} \tag{2}$$

with a suitable function f. For the derivation of f, measured stress–strain curves can be used, see, e.g., Stadler et al. (2019). Assuming that the bending load of the strip cross section x does not decrease (no unloading cycle), it is plastically deformed in the domain ② characterized by $|\kappa(x)| > \kappa_\mathrm{el}$. Assume now that the local bending load reaches an extremum at the point $(\kappa^*, m_\mathrm{b}^*)$ with $m_\mathrm{b}^* = f(\kappa^*)$. Here, the residual curvature can be computed as

$$\kappa_0(x) = \kappa^* + \frac{m_\mathrm{b}^*}{k_\mathrm{b}}. \tag{3}$$

After reaching this point, a linear elastic unloading and loading cycle ③ takes place. Here, the bending moment first evolves according to

$$m_\mathrm{b}(x) = -k_\mathrm{b}(\kappa(x) - \kappa_0(x)) \tag{4}$$

as long as $m_\mathrm{b}(x) \le m_\mathrm{b}^*$. Even if $m_\mathrm{b}(x) < 0$ occurs during ③, Eq. (4) is used because a plastic deformation in opposite direction is excluded. As soon as $m_\mathrm{b}(x) \ge m_\mathrm{b}^*$ is satisfied, the bending history switches back to the initial curve ④, where the residual curvature $\kappa_0(x)$ is continuously updated according to

$$\kappa_0(x) \leftarrow \kappa(x) + \frac{m_\mathrm{b}(x)}{k_\mathrm{b}}. \tag{5}$$

In summary, the constitutive law which also considers the bending history reads as

$$\kappa(x) = \begin{cases} m_{\mathrm{b,ic}}^{-1}(m_\mathrm{b}(x)) & \text{if } \kappa_0(x) = 0 \vee \\ & [(\kappa_0(x) < 0) \wedge (m_\mathrm{b}(x) \ge m_\mathrm{b}^*)] \vee \\ & [(\kappa_0(x) > 0) \wedge (m_\mathrm{b}(x) \le m_\mathrm{b}^*)] \\ \kappa_0(x) - \dfrac{m_\mathrm{b}(x)}{k_\mathrm{b}} & \text{if } [(\kappa_0(x) < 0) \wedge (m_\mathrm{b}(x) < m_\mathrm{b}^*)] \\ & \vee [(\kappa_0(x) > 0) \wedge (m_\mathrm{b}(x) > m_\mathrm{b}^*)]. \end{cases} \tag{6}$$

2.2. Quasi-static strip deformation model

The differential equation of the center line of the considered strip and the corresponding boundary conditions are formulated in the following. Acceleration forces are neglected because only slow roll movements are considered. The dead weight $g\rho h$ constitutes a uniformly distributed load on the strip, where $g = 9.81\,\mathrm{m/s^2}$ denotes the gravitational acceleration, and $\rho = 7850\,\mathrm{kg/m^3}$ is the mass density of steel. The tensional force n applied to the strip at $x = 0$ is another external load, see Fig. 2(a). The tensional force n is assumed to be uniform along the strip, (cf. Steinboeck et al., 2015). Moreover, linear geometric relations are considered and small deflections w are assumed. In the geometrically linear case (small deflections and strains), it is justified to approximate the curvature Eq. (1) by

$$\kappa(x) \approx w''(x). \tag{7}$$

Considering these assumptions, the momentum balance of the strip is defined by the differential equation

$$m_\mathrm{b}''(x) - g\rho h + n\kappa(x) = 0\ , \tag{8}$$

which is supplemented with appropriate boundary conditions. In case of an axially moving strip with a constant and spatially uniform velocity v, the right hand side of Eq. (8) needs to be replaced by the term $\rho h v^2 w''(x)$. This term represents centrifugal forces and is negligibly small for velocities v typically used in industrial furnaces. For a detailed derivation of this differential equation, see, e.g., Steinboeck et al. (2015). With Eqs. (7)-(8), the equilibrium condition $m_\mathrm{b}'(x) = q(x)$, where $q(x)$ describes the shear force in the strip cross section x, and the application of the Euler–Bernoulli hypothesis, the nonlinear first-order differential equation

$$\frac{\mathrm{d}}{\mathrm{d}x}\begin{bmatrix} w(x) \\ w'(x) \\ q(x) \\ m_\mathrm{b}(x) \end{bmatrix} = \begin{bmatrix} w'(x) \\ \kappa(x) \\ g\rho h - n\kappa(x) \\ q(x) \end{bmatrix}, \quad x \in (0, L) \tag{9}$$

can be formulated, (cf. Stadler et al., 2017). The boundary conditions at the known boundaries $x = 0$, $x = L$, and at the generally unknown strip-roll contact point $x = x_\mathrm{cp}$ read as

$$w(0) = 0, \qquad w'(0) = 0 \tag{10a}$$

$$w(L) = 0, \qquad w'(L) = 0 \tag{10b}$$

$$w(x_\mathrm{cp}^-) = w(x_\mathrm{cp}^+), \qquad w'(x_\mathrm{cp}^-) = w'(x_\mathrm{cp}^+) \tag{10c}$$

$$m_\mathrm{b}(x_\mathrm{cp}^-) = m_\mathrm{b}(x_\mathrm{cp}^+), \qquad w'(x_\mathrm{cp}) = \frac{x_\mathrm{r} - x_\mathrm{cp}}{\sqrt{R^2 - (x_\mathrm{r} - x_\mathrm{cp})^2}} \tag{10d}$$

$$w(x_\mathrm{cp}) = z_\mathrm{r} - R + \sqrt{R^2 - (x_\mathrm{cp} - x_\mathrm{r})^2}. \tag{10e}$$

Here, x_cp^+ and x_cp^- denote the right- and the left-hand limit at the strip-roll contact point x_cp, respectively. The contact condition, that is the equations for $w(x_\mathrm{cp})$ and $w'(x_\mathrm{cp})$ in Eq. (10), ensures that the slopes of the roll and the strip are consistent at the strip-roll contact point x_cp. Since x_cp is not known, the condition (10e) is added to the system, which relates the strip deflection w with the control inputs x_r and z_r.

For the model to store, update, and evaluate the residual curvature κ_0 at an arbitrary point x, the strip is equidistantly discretized into N_bh grid points in longitudinal direction. The residual curvature is consequently stored at these nodes. For the numeric integration of Eq. (9), the nodal values of κ_0 are linearly interpolated between the nodes. To solve the nodal model Eqs. (9)-(10), the boundary value problem solver `bvpsol` (multiple shooting approach) was used, see Deuflhard (2004) for more details.

3. Controller design

The considered control task is to realize a desired trajectory (parameterized in $x_\mathrm{r}(t)$) of the contact force $q_\mathrm{cp}^\mathrm{d}(t)$ and the curvature $\kappa_\mathrm{cp}^\mathrm{d}(t)$ at the strip-roll contact point $x_\mathrm{cp}(t)$. To perform this task, a 2-DOF control structure, consisting of a feedforward and a feedback part, according to

$$\mathbf{u}(t) = \begin{bmatrix} n(t) \\ z_\mathrm{r}(t) \end{bmatrix} = \mathbf{u}_\mathrm{ff}(t) + \Delta\mathbf{u}(t) \tag{11}$$

is proposed. Here, $n(t)$ is the tensional force and $z_\mathrm{r}(t)$ is the penetration depth of the roll. Ideally, in such a control structure, the dominant part of the control input $\mathbf{u}(t)$ is contributed by the feedforward controller $\mathbf{u}_\mathrm{ff}(t)$, while unknown disturbances and model-plant mismatches (such as uncertainties in the constitutive law $m_\mathrm{b}(\kappa)$, an inhomogeneous strip thickness h, or an inhomogeneous and unknown initial residual curvature $\kappa_0(x) \neq 0$) are compensated for by the feedback controller $\Delta\mathbf{u}(t)$. For the controller design, the horizontal position $x_\mathrm{r}(t)$ of the roll is considered to be a given (operator-defined) periodic input trajectory. The low absolute velocity $|v_\mathrm{r}(t)|$ of the roll justifies the assumption of a quasi-static process.

3.1. Feedforward control

For a given input trajectory $\mathbf{u}(t)$ and known $x_\mathrm{r}(t)$ and $\kappa_0(x)$, the quasi-static solution of Eqs. (9)-(10) can be formally written as a nonlinear functional $\boldsymbol{\Upsilon}$ in the form

$$\begin{aligned} \mathbf{y}(t) &= \begin{bmatrix} q_\mathrm{cp}(t) \\ \kappa_\mathrm{cp}(t) \end{bmatrix} = \begin{bmatrix} q(x_\mathrm{cp}^-) - q(x_\mathrm{cp}^+) \\ \kappa(x_\mathrm{cp}) \end{bmatrix} \\ &= \boldsymbol{\Upsilon}(t, \mathbf{u}(\tau), x_\mathrm{r}(\tau), \kappa_0(x)|_{t=0})\ , \quad \tau \in [0, t]. \end{aligned} \tag{12}$$

Because an initially plain strip is considered, $\kappa_0(x) = 0\ \forall x$ at time $t = 0$. It is worth noting that this is no restriction of generality. The proposed approach is also applicable for $\kappa_0(x)|_{t=0} \neq 0$. Evaluating Eq. (12) at the desired nominal operating point gives

$$\mathbf{y}^\mathrm{d}(t) = \begin{bmatrix} q_\mathrm{cp}^\mathrm{d}(t) \\ \kappa_\mathrm{cp}^\mathrm{d}(t) \end{bmatrix} = \boldsymbol{\Upsilon}(t, \mathbf{u}_\mathrm{ff}(\tau), x_\mathrm{r}(\tau), 0)\ , \quad \tau \in [0, t]. \tag{13}$$

This relation is numerically solved using Newton's method. Formally, this yields the feedforward control law

$$\mathbf{u}_\mathrm{ff}(t) = \begin{bmatrix} n_\mathrm{ff}(t) \\ z_\mathrm{r,ff}(t) \end{bmatrix} = \boldsymbol{\Upsilon}^{-1}(t, \mathbf{y}^\mathrm{d}(\tau), x_\mathrm{r}(\tau), 0)\ , \quad \tau \in [0, t] \tag{14}$$

for given desired trajectories $x_\mathrm{r}(t)$ and $\mathbf{y}^\mathrm{d}(t)$. In practical terms, the computation of Eq. (14) is carried out for a discretized time axis with the step size Δt. In essence, Δt is chosen small enough so that the resulting change of $\kappa_0(x)$ in each time step is sufficiently small and below a certain threshold. Furthermore, $\kappa_0(x)$ is assumed to be constant within each time step and is only updated at the end of each sampling period. The feedforward control input $\mathbf{u}_\mathrm{ff}(t)$ can be computed off-line since the desired output trajectory $\mathbf{y}^\mathrm{d}(t)$ is specified by the operator in advance.

At the top of Fig. 4, a typical computed feedforward control input trajectory $\mathbf{u}_\mathrm{ff}(t)$ is shown. In this scenario, the roll periodically moves from $x_\mathrm{r} = 0.58\,\mathrm{m}$ to $x_\mathrm{r} = 1.17\,\mathrm{m}$ and vice versa. Furthermore, T_ILC is the time span it takes the roll to move between these positions.

A constant curvature $\kappa_\mathrm{cp}^\mathrm{d}(t) = -1.25/\mathrm{m}$ and a constant contact force $q_\mathrm{cp}^\mathrm{d}(t) = 200\,\mathrm{N/m}$ are the desired output trajectories for all roll positions $x_\mathrm{r}(t) \in (0.58\,\mathrm{m}, 1.17\,\mathrm{m})$. After a few cycles ($t/T_\mathrm{ILC} \geq 4$), the computed trajectories become periodic (the residual curvature $\kappa_0(x)$ does not change any more). Hence, it is assumed in the following that only scenarios are considered which exhibit a periodic solution. This behavior can be exploited for the design of an iterative learning control strategy, which will be presented in Section 3.2.2.

The bottom part of Fig. 4 shows snapshots of the curvature $\kappa(x)$ and the residual curvature $\kappa_0(x)$ of the strip at discrete times t/T_ILC.

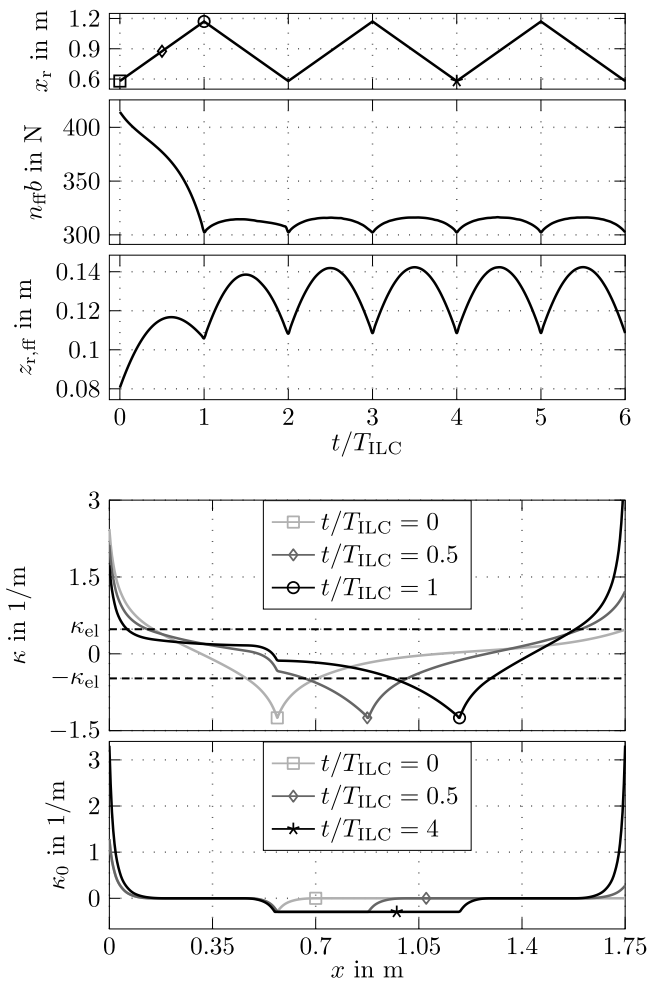

Fig. 4. Computed open-loop control inputs $n_{ff}(t)$ and $z_{r,ff}(t)$ for a periodic trajectory $x_r(t) \in [0.58\,\text{m}, 1.17\,\text{m}]$, a constant curvature $\kappa_{cp}^{d}(t) = -1.25/\text{m}$, and a constant contact force $q_{cp}^{d}(t) = 200\,\text{N/m}$ (top). Curvature $\kappa(x)$ and residual curvature $\kappa_0(x)$ of the strip at discrete times t/T_{ILC} (bottom).

In this setting, $t = 0$ designates the point in time where the computed control input trajectory $\mathbf{u}_{ff}(t)$ has already been applied to the initially plain strip (i.e., $\kappa_0(x) = 0\ \forall x$) and results in a plastic deformation of the strip. Hence, the bottom graph in Fig. 4 shows a non-zero residual curvature $\kappa_0(x)$ at $t/T_{ILC} = 0$. Furthermore, only the case $z_r > 0$, $\kappa_{cp} < 0$, and thus $\kappa_0(x) \leq 0$ in the vicinity of the strip-roll contact point can occur. As can be seen in Fig. 4, $\kappa(x) > \kappa_{el}$, which entails $\kappa_0(x) > 0$, only emerges near the boundaries $x = 0$ and $x = L$. The distributions of the curvature $\kappa(x)$ in Fig. 4 confirm that once a strip cross section x is plastically deformed, $\text{sgn}(\kappa_0(x))$ remains constant at this cross section. This justifies the assumption that there is no plastic deformation in opposite direction, cf. Section 2.1.

3.2. Feedback control

The feedforward control input $\mathbf{u}_{ff}(t)$ is not able to suppress deviations from the desired output trajectories caused by model-plant mismatches or disturbances. Therefore, an additional feedback controller is introduced. As shown in Section 3.1, a fixed periodic roll movement $x_r(t)$ and a periodic reference signal $\mathbf{y}^{d}(t)$, which is periodic with respect to $x_r(t)$, leads to a periodic feedforward control input $\mathbf{u}_{ff}(t)$ and constant values $\kappa_0(x)$ after a few iterations. Under these conditions, a feedback controller can be derived based on a linearization of the model about the periodic steady state feedforward solution. Let $\mathbf{u}_{ff}^{per}(t)$ denote the periodic steady state of the feedforward control input $\mathbf{u}_{ff}(t)$ and $\boldsymbol{\Upsilon}^{per}$ the corresponding input/output relation given by Eq. (12) in the form

$$\mathbf{y}^{d}(t) = \boldsymbol{\Upsilon}^{per} = \boldsymbol{\Upsilon}\left(t, \mathbf{u}_{ff}^{per}(\tau), x_r(\tau), 0\right)\ , \quad \tau \in [0, t]. \tag{15}$$

Note that Eq. (15) is evaluated for $t \gg$, i.e. for times when the change in the residual curvature is sufficiently small and thus the periodic state is achieved. In contrast to $\boldsymbol{\Upsilon}$, $\boldsymbol{\Upsilon}^{per}$ does not represent a functional but rather a function because the residual curvature $\kappa_0(x)$ is constant with respect to the time t for $\boldsymbol{\Upsilon}^{per}$. Furthermore, the time t is mapped to the current horizontal roll position $x_r(t)$ according to

$$x_r(t) = \int_0^t v_r(\tau)\,\mathrm{d}\tau\ , \tag{16}$$

with the horizontal roll velocity $v_r(t)$. For $t \in (0, T_{ILC})$, this spatial mapping is one-to-one as long as $\text{sgn}(v_r(t)) = \text{const.} \wedge v_r(t) \neq 0$ holds for all $t \in (0, T_{ILC})$. Using Eq. (16) and for small deviations $\Delta\mathbf{u}(t)$ from $\mathbf{u}_{ff}^{per}(t)$, this results in

$$\mathbf{y}(t) = \mathbf{y}^{d}(t) + \Delta\mathbf{y}(t) \tag{17}$$

with the linearized time-varying mapping

$$\Delta\mathbf{y}(t) = \underbrace{\left.\frac{\partial\boldsymbol{\Upsilon}^{per}}{\partial\mathbf{u}_{ff}^{per}}\right|_{x_r(t)}}_{\mathbf{A}(x_r(t))}\Delta\mathbf{u}(t). \tag{18}$$

In the following sections, a control strategy consisting of a multivariable PI controller and a spatial ILC in the form

$$\Delta\mathbf{u}(t) = \Delta\mathbf{u}_{fb}(t) + \Delta\mathbf{u}_{ILC}(t) \tag{19}$$

is developed. This combined approach allows for an effective suppression of recurring as well as non-recurring disturbances.

3.2.1. Multivariable PI control

Given the linearized model Eq. (18), it is reasonable to choose a multivariable PI output feedback controller according to

$$\frac{\mathrm{d}}{\mathrm{d}t}\mathbf{e}_I(t) = \Delta\mathbf{y}(t) = \mathbf{y}(t) - \mathbf{y}^{d}(t) \tag{20a}$$

$$\Delta\mathbf{u}_{fb}(t) = -\mathbf{A}^{-1}(x_r(t))\left(\mathbf{K}_P\Delta\mathbf{y}(t) + \mathbf{K}_I\mathbf{e}_I(t)\right). \tag{20b}$$

Note that $\mathbf{A}^{-1}(x_r(t))$ is non-singular for all considered points in the operating range. The use of $\mathbf{A}^{-1}(x_r(t))$ in Eq. (20b) ensures an approximate decoupling between the contact force Δq_{cp} and the curvature $\Delta\kappa_{cp}$. Furthermore, the exponential stability of the closed-loop system is guaranteed as long as $\mathbf{K}_P$ and $\mathbf{K}_I$ are chosen sufficiently small and $\mathbf{K}_I$ is a positive definite matrix, (cf. Korn & Jumar, 1991; Lunze, 1989).

3.2.2. Combined iterative learning and PI control

While the PI control law (20b) is a practicable way to reduce the control error, it cannot systematically cancel periodic disturbances (e.g. actuator backlash, friction, model-plant mismatches in the calculation of the feedforward control input). This drawback as well as the periodic inputs for periodic output reference trajectories suggest the augmentation of the feedback controller by an iterative or repetitive learning control technique. These learning control techniques can improve the control performance of a recurring process by learning based on previous iterations (trials), (cf. Ahn, Chen, & Moore, 2007; Ahn, Moore, & Chen, 2007; Bien & Xu, 1998; Bristow et al., 2006; Owens & Hätönen, 2005). The plant and the recurring process satisfy the following conditions:

1. Every iteration has the same fixed length.
2. Every iteration starts from the same initial condition.
3. For a desired output $\mathbf{y}^{d}(t)$, $t \in [0, T_{ILC}]$, there exists a unique control input $\mathbf{u}^{d}(t)$.

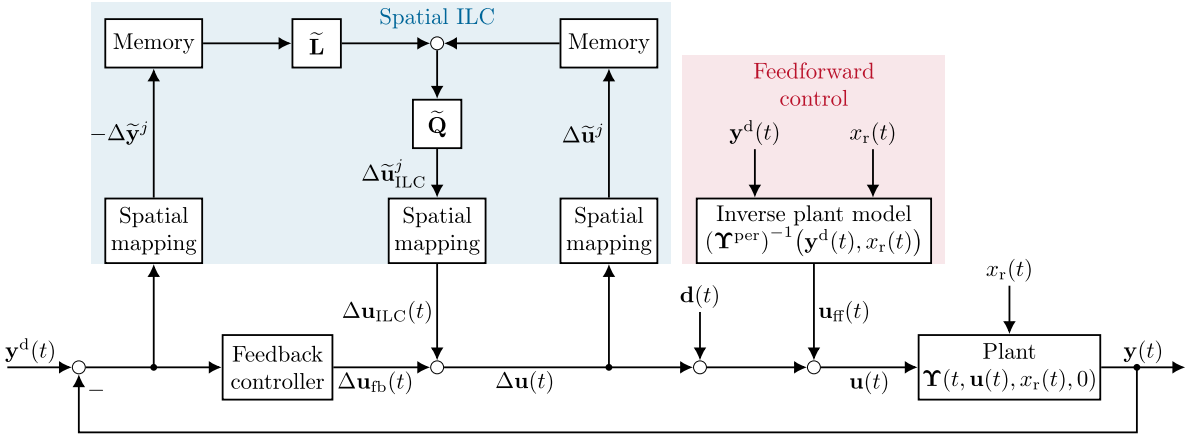

Fig. 5. Block diagram of the proposed combined ILC and PI control structure.

In this context, two learning techniques, i.e. ILC and repetitive control (RC), are distinguished in the literature, see, e.g., Insam et al. (2021). Under certain circumstances, ILC and RC are even equivalent, see, e.g., Freeman et al. (2013) and Roover et al. (2000). For ILC, all iterations are independent from each other, whereas they are dependent in the case of RC. For RC, typically the final state of the previous iteration is the initial state of the next iteration. For the considered system, it can be ensured that the initial states of the iterations are nearly identical (cf. Section 4.2). Thus, an ILC is proposed in the following. In principle, RC could also be used. This would avoid that the roll has to be stopped between iterations until the PI controller ensures convergence to the predefined initial state. The chosen ILC structure allows for the suppression of unwanted effects (e.g. static friction), since the PI feedback controller is active between iterations. In contrast, by using a repetitive controller, such effects would need to be corrected for during the course of the next trajectory.

The tracking performance of the ILC should be (approximately) independent of the specific shape of the trajectory $x_{\mathrm{r}}(t)$. To this end, the devised learning law will be formulated as a spatial ILC, see, e.g., Mahawan and Luo (2000), Marko et al. (2020), Wang et al. (2018) and Wijdeven and Bosgra (2010). To account for recurring and non-recurring disturbances, the ILC scheme should operate in conjunction with the PI feedback controller. While the plant mapping Eq. (18) is spatially invariant and thus independent of the specific trajectory $x_{\mathrm{r}}(t)$, the consideration of the PI feedback controller dynamics during the design of the ILC would result in a spatially varying mapping. This would be detrimental to the design goal of keeping the ILC independent of the specific trajectory $x_{\mathrm{r}}(t)$. To resolve this issue, a disturbance-observer-based ILC is used in this work, (cf. Chen & Tomizuka, 2014; Maeda et al., 2015). Combined with the ideas from spatial ILC, the ILC update is split into a spatial disturbance estimator and a suitable feedforward compensator of the estimated disturbance. The block diagram in Fig. 5 shows the suggested combined ILC and PI control structure. Its components will be described in the following sections.

3.2.3. Spatial mapping and lifted system description

In the following, the superscript $j = 0, 1, \dots$ denotes the iteration index of the ILC. Each iteration has the spatial length $L_{\mathrm{ILC}} = \max(x_{\mathrm{r}}(t)) - \min(x_{\mathrm{r}}(t))$ and consists of N_{ILC} nodes. Furthermore, all signals are discretized along the spatial coordinate $x \in (\min(x_{\mathrm{r}}(t)), \max(x_{\mathrm{r}}(t)))$ at the grid points kx_{g}, $k = 0, 1, \dots, N_{\mathrm{ILC}} - 1$ with the uniform step size x_{g}. E.g., $n^j[k]$, $k = 0, 1, \dots, N_{\mathrm{ILC}} - 1$ denotes the tensional force at iteration j and the grid point kx_{g}.

Considering also the generally unknown disturbance $\mathbf{d}(t)$, cf. Fig. 5, the linearized input/output relation (18) can be extended in the form

$$\Delta\widetilde{\mathbf{y}}^j = \widetilde{\mathbf{A}}\left(\Delta\widetilde{\mathbf{u}}^j + \widetilde{\mathbf{d}}\right), \tag{21}$$

where

$$\Delta\widetilde{\mathbf{y}}^j = \left[\Delta\mathbf{y}^j[0]^{\mathrm{T}} \quad \Delta\mathbf{y}^j[x_{\mathrm{g}}]^{\mathrm{T}} \quad \cdots \quad \Delta\mathbf{y}^j[x_{\mathrm{g}}(N_{\mathrm{ILC}}-1)]^{\mathrm{T}}\right]^{\mathrm{T}} \tag{22a}$$

$$\Delta\widetilde{\mathbf{u}}^j = \left[\Delta\mathbf{u}^j[0]^{\mathrm{T}} \quad \Delta\mathbf{u}^j[x_{\mathrm{g}}]^{\mathrm{T}} \quad \cdots \quad \Delta\mathbf{u}^j[x_{\mathrm{g}}(N_{\mathrm{ILC}}-1)]^{\mathrm{T}}\right]^{\mathrm{T}} \tag{22b}$$

$$\widetilde{\mathbf{d}} = \left[\mathbf{d}[0]^{\mathrm{T}} \quad \mathbf{d}[x_{\mathrm{g}}]^{\mathrm{T}} \quad \cdots \quad \mathbf{d}[x_{\mathrm{g}}(N_{\mathrm{ILC}}-1)]^{\mathrm{T}}\right]^{\mathrm{T}} \tag{22c}$$

denote the linearized output $\Delta\widetilde{\mathbf{y}}^j$, the linearized control input $\Delta\widetilde{\mathbf{u}}^j$, and the disturbance $\widetilde{\mathbf{d}}$ represented in lifted system form, cf. Owens (2016), respectively. Furthermore,

$$\widetilde{\mathbf{A}} = \operatorname{diag}\left(\mathbf{A}(0), \mathbf{A}(x_{\mathrm{g}}), \dots, \mathbf{A}(x_{\mathrm{g}}(N_{\mathrm{ILC}}-1))\right). \tag{23}$$

3.2.4. Disturbance-observer-based ILC

Two approaches will be considered in the derivation of the disturbance-observer-based ILC update. To this end, the disturbance estimate $\widetilde{\mathbf{d}}^j_{\mathrm{est}}$ at iteration j is obtained as the solution of the minimization problem

$$\min_{\widetilde{\mathbf{d}}^j_{\mathrm{est}}} J_{\mathrm{est}} = \frac{1}{2}\left\|\Delta\widetilde{\mathbf{y}}^j - \widetilde{\mathbf{A}}\left(\Delta\widetilde{\mathbf{u}}^j + \widetilde{\mathbf{d}}^j_{\mathrm{est}}\right)\right\|^2_{\mathbf{V}} + \frac{1}{2}\left\|\widetilde{\mathbf{d}}^j_{\mathrm{est}} + \Delta\widetilde{\mathbf{u}}^j\right\|^2_{\boldsymbol{\Gamma}}. \tag{24}$$

Here, $\mathbf{V} = \operatorname{diag}([v_1, v_2, v_1, v_2, \dots]) \in \mathbb{R}^{2N_{\mathrm{ILC}}\times 2N_{\mathrm{ILC}}}$ and $\boldsymbol{\Gamma} = \operatorname{diag}([\gamma_1, \gamma_2, \gamma_1, \gamma_2, \dots]) \in \mathbb{R}^{2N_{\mathrm{ILC}}\times 2N_{\mathrm{ILC}}}$ are positive definite weighting matrices and $\|\cdot\|^2_{\mathbf{V}}$, $\|\cdot\|^2_{\boldsymbol{\Gamma}}$ denote the weighted 2-norm with the weights $\mathbf{V}$ and $\boldsymbol{\Gamma}$, respectively. For fixed values $\Delta\widetilde{\mathbf{u}}^j$ and $\Delta\widetilde{\mathbf{y}}^j$, Eq. (24) is quadratic in $\widetilde{\mathbf{d}}_{\mathrm{est}}$. Thus, it constitutes a convex optimization problem with a single (global) optimum. The first term in Eq. (24) refers to a model-based disturbance estimator and the second term aims at taking the disturbance estimate for the next iteration simply as the negative control input $\Delta\widetilde{\mathbf{u}}^j$ during the previous iteration. The rational behind this second term is that the PI feedback controller already achieves some amount of disturbance attenuation. The ILC simply memorizes the control input which leads to this disturbance attenuation and reuses it during the next iteration. The minimization problem in Eq. (24) yields the explicit solution

$$\widetilde{\mathbf{d}}^j_{\mathrm{est}} = -\Delta\widetilde{\mathbf{u}}^j + \left(\boldsymbol{\Gamma} + \widetilde{\mathbf{A}}^{\mathrm{T}}\mathbf{V}\widetilde{\mathbf{A}}\right)^{-1}\widetilde{\mathbf{A}}^{\mathrm{T}}\mathbf{V}\Delta\widetilde{\mathbf{y}}^j. \tag{25}$$

ILC disturbance rejection is then realized by the feedforward term

$$\begin{aligned}\Delta\widetilde{\mathbf{u}}^{j+1}_{\mathrm{ILC}} = -\widetilde{\mathbf{d}}^j_{\mathrm{est}} &= \Delta\widetilde{\mathbf{u}}^j - \left(\boldsymbol{\Gamma} + \widetilde{\mathbf{A}}^{\mathrm{T}}\mathbf{V}\widetilde{\mathbf{A}}\right)^{-1}\widetilde{\mathbf{A}}^{\mathrm{T}}\mathbf{V}\Delta\widetilde{\mathbf{y}}^j \\ &= \Delta\widetilde{\mathbf{u}}^j - \widetilde{\mathbf{L}}\Delta\widetilde{\mathbf{y}}^j,\end{aligned} \tag{26}$$

with the learning gain

$$\widetilde{\mathbf{L}} = \left(\boldsymbol{\Gamma} + \widetilde{\mathbf{A}}^{\mathrm{T}}\mathbf{V}\widetilde{\mathbf{A}}\right)^{-1}\widetilde{\mathbf{A}}^{\mathrm{T}}\mathbf{V}. \tag{27}$$

To prevent learning at high frequencies, Eq. (26) is augmented by a low-pass filter. This results in

$$\Delta\widetilde{\mathbf{u}}^{j+1}_{\mathrm{ILC}} = \widetilde{\mathbf{Q}}\left(\Delta\widetilde{\mathbf{u}}^j - \widetilde{\mathbf{L}}\Delta\widetilde{\mathbf{y}}^j\right), \tag{28}$$

Table 1
Parameters of the considered laboratory experiment.

Description	Parameter	Value	Unit
Width of strip A and B	b	150	mm
Thickness of strip A	h	1.98	mm
Thickness of strip B	h	1.25	mm
Weighting parameter	γ_1	$1 \cdot 10^{-9} \div 1 \cdot 10^{-8}$	m^2/N^2
Weighting parameter	γ_2	$1 \cdot 10^{-9} \div 1 \cdot 10^{-8}$	$1/m^2$
Weighting parameter	υ_1	1	m^2/N^2
Weighting parameter	υ_2	1	m^2
Roll radius	R	150	mm
Length of the strip	L	1.75	m

where $\widetilde{\mathbf{Q}}$ is a suitable Q-filter matrix (its design will be discussed later). Note that the suggested ILC update law (26) depends on the total control input $\Delta\widetilde{\mathbf{u}}^j$, and therefore differs from a conventional ILC, where $\Delta\widetilde{\mathbf{u}}^{j+1}_{\mathrm{ILC}} = \Delta\widetilde{\mathbf{u}}^{j}_{\mathrm{ILC}} - \widetilde{\mathbf{L}}\Delta\widetilde{\mathbf{y}}^j$ would be used. Considering Eqs. (19) and (21), the total control input $\Delta\widetilde{\mathbf{u}}^j$, combining the PI controller (which is reset after each iteration) and the ILC is given by

$$\begin{aligned}\Delta\widetilde{\mathbf{u}}^j &= \Delta\widetilde{\mathbf{u}}^j_{\mathrm{fb}} + \Delta\widetilde{\mathbf{u}}^j_{\mathrm{ILC}} = -\widetilde{\mathbf{R}}\Delta\widetilde{\mathbf{y}}^j + \Delta\widetilde{\mathbf{u}}^j_{\mathrm{ILC}} \\ &= \underbrace{\left(\mathbf{I}+\widetilde{\mathbf{R}}\widetilde{\mathbf{A}}\right)^{-1}}_{\widetilde{\mathbf{S}}}\Delta\widetilde{\mathbf{u}}^j_{\mathrm{ILC}} - \underbrace{\left(\mathbf{I}+\widetilde{\mathbf{R}}\widetilde{\mathbf{A}}\right)^{-1}\widetilde{\mathbf{R}}\widetilde{\mathbf{A}}}_{\widetilde{\mathbf{T}}}\widetilde{\mathbf{d}}.\end{aligned} \tag{29}$$

Here, $\mathbf{I}$ is the identity matrix and the term $\Delta\widetilde{\mathbf{u}}^j_{\mathrm{fb}} = -\widetilde{\mathbf{R}}\Delta\widetilde{\mathbf{y}}^j$ represents the corresponding lifted system representation of the PI control law in Eq. (20). Using $\widetilde{\mathbf{T}} = \widetilde{\mathbf{S}}\widetilde{\mathbf{R}}\widetilde{\mathbf{A}}$ and $\widetilde{\mathbf{S}} = \mathbf{I} - \widetilde{\mathbf{T}}$ together with Eq. (21), Eq. (26) and Eq. (29) leads to

$$\Delta\widetilde{\mathbf{u}}^{j+1}_{\mathrm{ILC}} = \widetilde{\mathbf{Q}}(\mathbf{I}-\widetilde{\mathbf{L}}\widetilde{\mathbf{A}})\widetilde{\mathbf{S}}\Delta\widetilde{\mathbf{u}}^j_{\mathrm{ILC}} - \widetilde{\mathbf{Q}}\left(\widetilde{\mathbf{T}}+\widetilde{\mathbf{L}}\widetilde{\mathbf{A}}\widetilde{\mathbf{S}}\right)\widetilde{\mathbf{d}}\,, \tag{30}$$

which results in the monotonic convergence condition

$$\left\|\widetilde{\mathbf{Q}}(\mathbf{I}-\widetilde{\mathbf{L}}\widetilde{\mathbf{A}})\widetilde{\mathbf{S}}\right\|_2 < 1\,, \tag{31}$$

see also Maeda et al. (2015).

To get a better insight into the design of the minimization problem Eq. (24), the limiting cases $\boldsymbol{\Gamma}|_{\gamma_1\to\infty,\gamma_2\to\infty}$ ($\widetilde{\mathbf{L}} = \mathbf{0}$) and $\boldsymbol{\Gamma} = \mathbf{0}$ ($\widetilde{\mathbf{L}} = \widetilde{\mathbf{A}}^{-1}$, where $\widetilde{\mathbf{A}}$ is a non-singular matrix) will be discussed in further detail. For $\boldsymbol{\Gamma}|_{\gamma_1\to\infty,\gamma_2\to\infty}$, Eq. (28) simplifies to

$$\Delta\widetilde{\mathbf{u}}^{j+1}_{\mathrm{ILC}} = \widetilde{\mathbf{Q}}\left(\Delta\widetilde{\mathbf{u}}^j\right)\,, \tag{32}$$

i.e. prior knowledge of the dynamic matrix $\widetilde{\mathbf{A}}$ is not used in the ILC. In this case, the ILC solely learns based on the previous PI control actions, and the convergence criterion in Eq. (31) reduces to

$$\left\|\widetilde{\mathbf{Q}}\widetilde{\mathbf{S}}\right\|_2 < 1. \tag{33}$$

Hence, the choice of the Q-filter matrix is the only design freedom to ensure the convergence of the update law. For $\boldsymbol{\Gamma} = \mathbf{0}$ ($\widetilde{\mathbf{L}} = \widetilde{\mathbf{A}}^{-1}$), Eq. (31) becomes

$$\left\|\widetilde{\mathbf{Q}}(\mathbf{I}-\widetilde{\mathbf{L}}\widetilde{\mathbf{A}})\widetilde{\mathbf{S}}\right\|_2 = \left\|\widetilde{\mathbf{Q}}(\mathbf{I}-\mathbf{I})\widetilde{\mathbf{S}}\right\|_2 = \mathbf{0}. \tag{34}$$

This indicates the well-known one step convergence of the ILC for the learning gain matrix $\widetilde{\mathbf{L}} = \widetilde{\mathbf{A}}^{-1}$. In this case, an ideal plant inverse is realized.

3.2.5. Acausal filtering of the control inputs

To suppress non-repetitive disturbances and (high-frequency) measurement noise in the ILC, a Q-filter, e.g., a Gaussian filter, was introduced in Eq. (28). To obtain the entries of the Q-filter matrix, the use of the discretized Gaussian distribution

$$q_G[k] = \frac{1}{\sigma_q\sqrt{2\pi}}\exp\left(\frac{-(kx_g)^2}{2\sigma_q^2}\right) \tag{35}$$

is often suggested in the literature, (cf. Bristow et al., 2006). The standard deviation

$$\sigma_q = \frac{\sqrt{\ln(2)}}{2\pi f_q} \tag{36}$$

follows from the 3-dB bandwidth f_q of the Q-filter. Masking with a rectangular window of length $2N_q+1$ and normalizing yield the final filter coefficients

$$q_f[k] = \begin{cases} \dfrac{q_G[k]}{\sum_{m=-N_q}^{N_q} q_G[m]} & \text{if } |k| \le N_q,\ f \in \{n, z_{\mathrm{r}}\} \\ 0 & \text{else}\,. \end{cases} \tag{37}$$

The Q-filter matrix finally reads as

$$\widetilde{\mathbf{Q}} = \begin{bmatrix} q_n[0] & 0 & \cdots & q_n[-(\bar{N}-1)] & 0 \\ 0 & q_{z_{\mathrm{r}}}[0] & \cdots & 0 & q_{z_{\mathrm{r}}}[-(\bar{N}-1)] \\ q_n[1] & 0 & \cdots & q_n[-(\bar{N}-2)] & 0 \\ 0 & q_{z_{\mathrm{r}}}[1] & \cdots & 0 & q_{z_{\mathrm{r}}}[-(\bar{N}-2)] \\ \vdots & \vdots & \ddots & \vdots & \vdots \\ q_n[\bar{N}-1] & 0 & \cdots & q_n[0] & 0 \\ 0 & q_{z_{\mathrm{r}}}[\bar{N}-1] & \cdots & 0 & q_{z_{\mathrm{r}}}[0] \end{bmatrix} \tag{38}$$

with $\bar{N} = N_{\mathrm{ILC}}$. Note that the first and last $2N_q$ rows in Eq. (38) need to be adjusted in practice such that the respective row sums are one.

4. Laboratory experiment

This section presents measurement results from the experimental test rig shown in Fig. 2(b). The control strategy proposed in Section 3 was implemented and validated for two different steel strips, denoted as strip A and B. The relevant parameters of the laboratory experiment are listed in Table 1.

4.1. Measurement of the strip curvature

To measure the deflection of the strip, infrared markers are placed on the surface of the strip and their positions are tracked by a stereo-vision infrared camera system. The measured coordinates of the markers are collected in the vectors

$$\mathbf{x}_{\mathrm{ir}}(t) = \begin{bmatrix} x_{\mathrm{ir},1}(t) & x_{\mathrm{ir},2}(t) & \cdots & x_{\mathrm{ir},N_{\mathrm{ir}}}(t) \end{bmatrix}^{\mathrm{T}} \tag{39a}$$

$$\mathbf{z}_{\mathrm{ir}}(t) = \begin{bmatrix} z_{\mathrm{ir},1}(t) & z_{\mathrm{ir},2}(t) & \cdots & z_{\mathrm{ir},N_{\mathrm{ir}}}(t) \end{bmatrix}^{\mathrm{T}}\,, \tag{39b}$$

where N_{ir} denotes the number of infrared markers. Then, a Savitzky-Golay filter with non-equally spaced nodes is used to estimate the curvature of the strip, (cf. Press et al., 2007; Savitzky & Golay, 1964). The reason for using a Savitzky-Golay filter is its easy adjustability and real-time capability. Let the odd number l_{w} be the window length of the Savitzky-Golay filter and consider $\bar{l}_{\mathrm{w}} = \frac{l_{\mathrm{w}}-1}{2}$. Furthermore, let

$$\check{\mathbf{z}}_{\mathrm{ir},i} = \begin{bmatrix} z_{\mathrm{ir},i-\bar{l}_{\mathrm{w}}} & \cdots & z_{\mathrm{ir},i+\bar{l}_{\mathrm{w}}} \end{bmatrix}^{\mathrm{T}}, \quad i = 1+\bar{l}_{\mathrm{w}}, \dots, N_{\mathrm{ir}}-\bar{l}_{\mathrm{w}} \tag{40}$$

be the subvector of $\mathbf{z}_{\mathrm{ir}}$ that corresponds to the filter window. The filter locally approximates the deflection of the strip by a polynomial function of order m. For $l_{\mathrm{w}} > m+1$, this results in the approximation $\mathbf{X}_i\mathbf{p}_i$ of $\check{\mathbf{z}}_{\mathrm{ir},i}$, with the data matrix

$$\mathbf{X}_i = \begin{bmatrix} 1 & x_{\mathrm{ir},i-\bar{l}_{\mathrm{w}}} & \cdots & x^{m-1}_{\mathrm{ir},i-\bar{l}_{\mathrm{w}}} & x^{m}_{\mathrm{ir},i-\bar{l}_{\mathrm{w}}} \\ \vdots & \vdots & \ddots & \vdots & \vdots \\ 1 & x_{\mathrm{ir},i+\bar{l}_{\mathrm{w}}} & \cdots & x^{m-1}_{\mathrm{ir},i+\bar{l}_{\mathrm{w}}} & x^{m}_{\mathrm{ir},i+\bar{l}_{\mathrm{w}}} \end{bmatrix}, \tag{41}$$

and the polynomial coefficients $\mathbf{p}_i = \begin{bmatrix} p_{i,0} & p_{i,1} & \cdots & p_{i,m} \end{bmatrix}^{\mathrm{T}}$. Minimizing the residual $\check{\mathbf{z}}_{\mathrm{ir},i} - \mathbf{X}_i\mathbf{p}_i$ in a least-squares sense gives the estimate

$$\mathbf{p}_i = \left(\mathbf{X}_i^{\mathrm{T}}\mathbf{X}_i\right)^{-1}\mathbf{X}_i^{\mathrm{T}}\check{\mathbf{z}}_{\mathrm{ir},i}. \tag{42}$$

To avoid a phase shift, the Savitzky–Golay filter is evaluated at the center of the filter window. Hence, the estimated curvature of the strip at the point $x_{\mathrm{ir},i}$ reads as

$$\kappa_i(t) \approx \sum_{j=2}^{m} j(j-1)x^{j-2}_{\mathrm{ir},i}(t)p_{i,j}\,, \quad i = 1+\bar{l}_{\mathrm{w}}, \dots, N_{\mathrm{ir}}-\bar{l}_{\mathrm{w}}. \tag{43}$$

The strip-roll contact point x_{cp} is determined by minimizing the normal distance between the strip and the center of the roll. Finally, the curvature κ_{cp} at the strip-roll contact point is found by linear interpolation between the values $\kappa_i(t)$ at the two adjacent nodes.

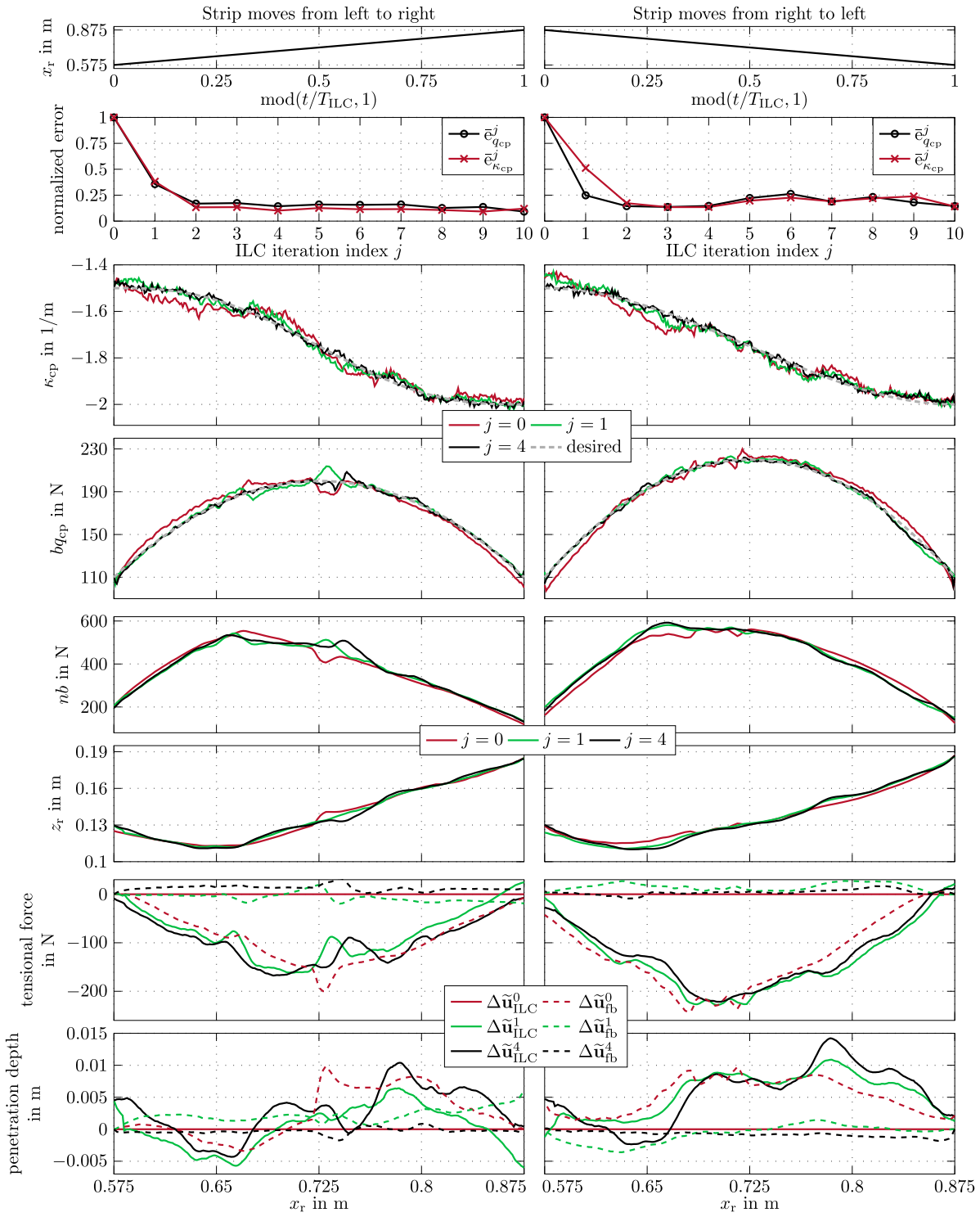

Fig. 6. Measurement results for strip A. Used parameters: $\gamma_1 = 10^{-8}\,\mathrm{m^2/N^2}$, $\gamma_2 = 10^{-8}\,\mathrm{m^{-2}}$, $f_q = 10/\mathrm{m}$, $N_q = 3$, $\mathbf{K}_I = \mathrm{diag}(0.4, 0.4)$.

4.2. Experimental results

During the conducted experiments, the roll was periodically moved between $x_r = 0.575\,\mathrm{m}$ and $x_r = 0.875\,\mathrm{m}$ with the constant absolute velocity v_r. Due to the plastic deformation of the strip, a new strip has to be used for each experiment. Therefore, to verify different output trajectories within one experiment, two different desired output trajectories are used for each movement direction of the roll. At iteration $j = 0$, only the feedforward control input $\mathbf{u}_{ff}$ and the PI control input $\Delta\mathbf{u}^0_{fb}$ are active while $\Delta\mathbf{u}^0_{ILC} = \mathbf{0}$. As stated in Section 3.2.2, every iteration must start from approximately the same initial condition. Hence, at the boundaries, the horizontal movement of the roll is interrupted until the PI controller achieves $\Delta\mathbf{y} \approx \mathbf{0}$. In the experiments, small values for γ_1 and γ_2, cf. Table 1, gave the best trade-off between convergence and robustness of the control. Moreover, increasing the proportional gain $\mathbf{K}_P$ of the PI controller from Eq. (20b) beyond a certain threshold induced significant vibrations of the test rig due to the dynamic limitations of the subordinate control loops (position control of the active slides). This problem was circumvented by choosing $\mathbf{K}_P = \mathbf{0}$ without sacrificing the control performance because the dominant part of the

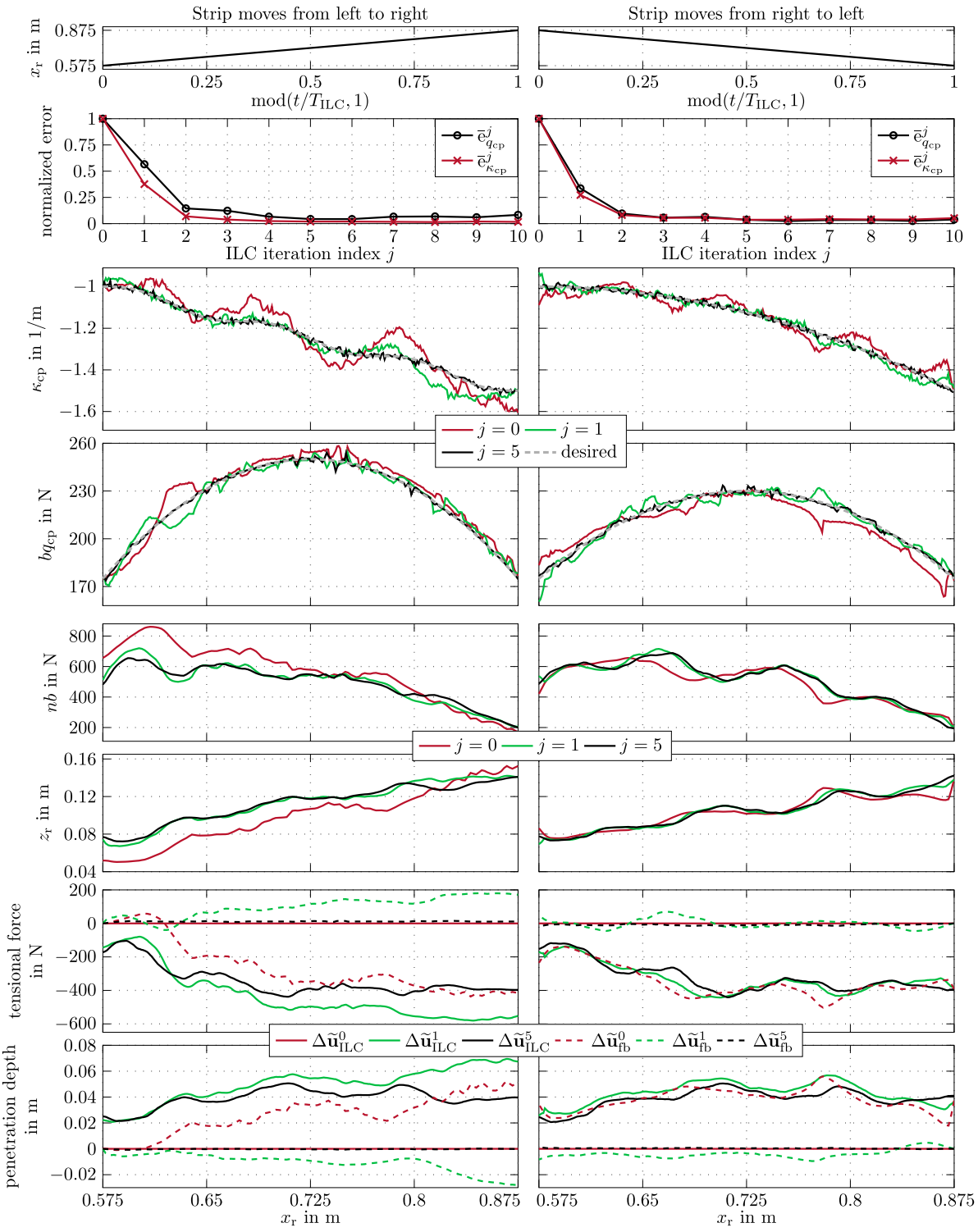

Fig. 7. Measurement results for strip B. Used parameters: $\gamma_1 = 10^{-9}\,\mathrm{m^2/N^2}$, $\gamma_2 = 10^{-9}\,\mathrm{m^{-2}}$, $f_q = 8/\mathrm{m}$, $N_q = 6$, $\mathbf{K}_I = \mathrm{diag}(0.2, 0.2)$.

feedback control signal $\Delta\tilde{\mathbf{u}}^j$ is contributed by the ILC and the objective of the PI controller is mainly to reject small local disturbances.

Figs. 6 and 7 show the measurement results for strips A and B, respectively. Strip B is substantially thinner than strip A, see Table 1. The second row of each figure shows the normalized mean squared errors

$$\bar{\mathrm{e}}^j_y = \frac{1}{\mathrm{e}^0_y N_{\mathrm{ILC}}} \sum_{k=0}^{N_{\mathrm{ILC}}-1} \left(y^{\mathrm{d}}[k] - y^j[k]\right)^2 \;,\; y \in \{\kappa_{\mathrm{cp}}, q_{\mathrm{cp}}\} \tag{44}$$

with

$$\mathrm{e}^0_y = \frac{1}{N_{\mathrm{ILC}}} \sum_{k=0}^{N_{\mathrm{ILC}}-1} \left(y^{\mathrm{d}}[k] - y^0[k]\right)^2 \;,\; y \in \{\kappa_{\mathrm{cp}}, q_{\mathrm{cp}}\} \tag{45}$$

for each iteration. The rows 3 and 4 show the controlled outputs $\mathbf{y}^j$ for several iterations and the rows 5 and 6 illustrate the corresponding control inputs $\mathbf{u}^j$. The rows 7 and 8 show the evolution of the feedback part $\Delta\mathbf{u}^j_{\mathrm{fb}}$ and the ILC part $\Delta\mathbf{u}^j_{\mathrm{ILC}}$. For both strips, the mean squared errors decrease significantly within the first few iterations and stay

within a tight range afterwards. This indicates that the steady state is already attained after a few iterations. Figs. 6 and 7 confirm that, while the control error is clearly recognizable in iteration $j = 0$ (no ILC contribution), the ILC quickly decreases the control error in the subsequent iterations and an excellent control performance is achieved at steady state. Clearly, this also reveals that the sole application of a PI feedback controller cannot achieve the desired tracking performance. The control inputs shown at the bottom of the figures demonstrate the intended behavior of the control strategy insofar as the ILC contributes the dominant part of the control input. The PI controller, in contrast, accounts for local disturbances and at steady state, its control signal is negligibly small compared to the ILC signal. The parameters f_q and N_q of the Gaussian filter, cf. Eq. (37), were manually adjusted for each strip. The same values f_q and N_q were used for both control input filters. As a general rule, thinner strips require filtering with a smaller bandwidth and a broader window size.

5. Summary and outlook

This paper presents a novel MIMO tracking control strategy for the contact force and the curvature at a strip-roll contact point. A quasi-static deformation model including a material model, which also considers the bending history of the strip, was derived. Based on this model, a MIMO 2-DOF control structure consisting of a feedforward and a feedback part was introduced. To track periodic output trajectories, the combination of a spatial ILC and a PI controller was utilized for the feedback part. The PI controller and the ILC can be independently designed and implemented due to the observer-based design strategy. This circumstance simplifies the industrial application since both controllers can be independently implemented, even on different target platforms. Moreover, the chosen ILC formulation allows to learn irrespective of the horizontal velocity of the roll and allows for a systematic suppression of periodic disturbances. In view of the industrial feasibility, the composition of rather simple control parts is also advantageous. E.g., the tuning of a PI controller is a well established process in industry and has been successfully mastered by many plant operators. The performance of the control structure was successfully validated on an experimental test rig. The insights gained from these laboratory studies can now be transferred to the industrial application to further study the evolution of surface defects on furnace rolls. Possible further research objectives concern the design of the ILC. Apart from the lifted system form, which entails a two-stage design process, a 2D systems formulation could also be used, where the ILC and the PI controller are designed in one step, see, e.g., Paszke et al. (2016).

Declaration of competing interest

The authors declare that they have no known competing financial interests or personal relationships that could have appeared to influence the work reported in this paper.

Acknowledgments

The financial support by the Austrian Federal Ministry for Digital and Economic Affairs, the National Foundation for Research, Technology and Development, the Christian Doppler Research Association, Austria and voestalpine Stahl GmbH, Austria is gratefully acknowledged. The authors acknowledge TU Wien Bibliothek, Austria for financial support through its Open Access Funding Programme.

References

Agarwal, K., Shivpuri, R., Zhu, Y., Chang, T.-S., & Huang, H. (2011). Process knowledge based multi-class support vector classification (PK-MSVM) approach for surface defects in hot rolling. *Expert Systems With Applications*, *38*(6), 7251–7262.

Ahn, H., Chen, Y., & Moore, K. (2007). Iterative learning control: brief survey and categorization. *IEEE Transactions On Systems, Man, And Cybernetics, Part C (Applications And Reviews)*, *37*(6), 1099–1121.

Ahn, H.-S., Moore, K. L., & Chen, Y. (2007). *Iterative learning control - Robustness and monotonic convergence for interval systems*. London: Springer.

Asano, K., Goto, T., Kohiro, Y., & Takahashi, H. (2007). Reel eccentricity control for reversing mills based on repetitive control. *IFAC Proceedings Volumes*, *40*(11), 299–304, 12th IFAC Symposium on Automation in Mining, Mineral and Metal Processing.

Basabe, V. V., & Szpunar, J. A. (2004). Growth rate and phase composition of oxide scales during hot rolling of low carbon steel. *ISIJ International*, *44*(9), 1554–1559.

Batty, F. A., & Lawson, K. (1965). Heavy plate levellers. *Journal Of The Iron And Steel Institute*, *203*, 1115–1128.

Bien, Z., & Xu, J.-X. (1998). *Iterative learning control - Analysis, design, integration and applications*. New York: Springer.

Brauneis, R., Steinboeck, A., Jochum, M., & Kugi, A. (2018). A robust real-time model for plate leveling. *IFAC-PapersOnLine*, *51*(2), 61–66.

Bristow, D. A., Tharayil, M., & Alleyne, A. (2006). A survey of iterative learning control. *IEEE Control Systems Magazine*, *26*(3), 96–114.

Chen, X., & Tomizuka, M. (2014). New repetitive control with improved steady-state performance and accelerated transient. *IEEE Transactions On Control Systems Technology*, *22*(2), 664–675.

Choi, I., Rossiter, J., & Fleming, P. (2007). Looper and tension control in hot rolling mills: A survey. *Journal Of Process Control*, *17*(6), 509–521.

Deuflhard, P. (2004). *Newton methods for nonlinear problems: Affine invariance and adaptive algorithms*. Berlin Heidelberg: Springer.

Freeman, C., Alsubaie, M., Cai, Z., Rogers, E., & Lewin, P. (2013). A common setting for the design of iterative learning and repetitive controllers with experimental verification. *International Journal Of Adaptive Control And Signal Processing*, *27*, 230–249.

Fukubayashi, H. H. (1995). Coating for high temperature pickup and wear resistant applications, thermal spraying: Current status and future trends. In *Proceedings of the 14th international thermal spray conference* (pp. 47–52). Kobe, Japan: High Temperature Society of Japan.

Garimella, S. S., & Srinivasan, K. (1994). Application of repetitive control to eccentricity compensation in rolling. *3*, In *Proceedings Of 1994 American control conference* (pp. 2904–2908).

Gopinath, S., & Kar, I. (2004). Iterative learning control scheme for manipulators including actuator dynamics. *Mechanism And Machine Theory*, *39*(12), 1367–1384.

Grüber, M., Kümmel, L., & Hirt, G. (2020). Control of residual stresses by roller leveling with regard to process stability and one-sided surface removal. *Journal Of Materials Processing Technology*, *280*, Article 116600.

Insam, C., Kist, A., Schwalm, H., & Rixen, D. J. (2021). Robust and high fidelity real-time hybrid substructuring. *Mechanical Systems And Signal Processing*, *157*, Article 107720.

Jin, N., Zhou, S., & Chang, T.-S. (2004). Identification of impacting factors of surface defects in hot rolling processes using multi-level regression analysis. *Transactions Of The North American Manufacturing Research Institute Of SME*, *32*, 557–564.

Kaiser, R., Hatzenbichler, T., Buchmayr, B., & Antretter, T. (2014). Simulation of the roller straightening process with respect to residual stresses and the curvature trend. In *Materials science forum: vol. 768, Proceedings of the international conference on residual stresses, vol. 9* (pp. 456–463).

Ketelhut, M., Stemmler, S., Gesenhues, J., Hein, M., & Abel, D. (2019). Iterative learning control of ventricular assist devices with variable cycle durations. *Control Engineering Practice*, *83*, 33–44.

Korn, U., & Jumar, U. (1991). *PI-Mehrgrößenregler*. München: Oldenbourg-Verlag.

Lankford, W. T. (1985). *The making, shaping, and treating of steel* (10th ed.). Pennsylvania: Association of Iron and Steel Engineers.

Lunze, J. (1989). *Robust multivariable feedback control* (1st ed.). New Jersey: Prentice-Hall.

Maeda, G. J., Manchester, I. R., & Rye, D. C. (2015). Combined ILC and disturbance observer for the rejection of near-repetitive disturbances, with application to excavation. *IEEE Transactions On Control Systems Technology*, *23*(5), 1754–1769.

Mahawan, B., & Luo, Z.-H. (2000). Repetitive control of tracking systems with time-varying periodic references. *International Journal Of Control*, *73*(1), 1–10.

Manayathara, T. J., Tsao, T. C., & Bentsman, J. (1996). Rejection of unknown periodic load disturbances in continuous steel casting process using learning repetitive control approach. *IEEE Transactions On Control Systems Technology*, *4*(3), 259–265.

Marko, L., Saxinger, M., Bittner, M., Steinboeck, A., & Kugi, A. (2020). Discrete-time repetitive control for multi-harmonic reference trajectories with arbitrary frequency. *IFAC-PapersOnLine*, *53*(2), 1646–1651.

Matthews, S., & James, B. (2010). Review of thermal spray coating applications in the steel industry: Part 1 – hardware in steel making to the continuous annealing process. *Journal Of Thermal Spray Technology*, *19*(6), 1267–1276.

Min, K., Kim, K., Kim, S. K., & Lee, D. (2012). Effects of oxide layers on surface defects during hot rolling processes. *Metals And Materials International*, *18*(2), 341–348.

Moir, S., & Preston, J. (2002). Surface defects—evolution and behaviour from cast slab to coated strip. *Journal Of Materials Processing Technology*, *125–126*, 720–724.

Munther, P. A., & Lenard, J. G. (1999). The effect of scaling on interfacial friction in hot rolling of steels. *Journal Of Materials Processing Technology*, *88*(1), 105–113.

Niederer, M., Strommer, S., Steinboeck, A., & Kugi, A. (2016). Nonlinear model predictive control of the strip temperature in an annealing furnace. *Journal Of Process Control*, *48*, 1–13.

Nioi, M., Celotto, S., Pinna, C., Swart, E., & Ghadbeigi, H. (2017). Surface defect evolution in hot rolling of high-Si electrical steels. *Journal Of Materials Processing Technology*, *249*, 302–312.

Nioi, M., Pinna, C., Celotto, S., Swart, E., Farrugia, D., Husain, Z., & Ghadbeigi, H. (2019). Finite element modelling of surface defect evolution during hot rolling of silicon steel. *Journal Of Materials Processing Technology*, *268*, 181–191.

Owens, D. H. (2016). *Iterative learning control: An optimization paradigm*. London, Springer.

Owens, D. H., Freeman, C. T., & Chu, B. (2013). Multivariable norm optimal iterative learning control with auxiliary optimisation. *International Journal Of Control*, *86*(6), 1026–1045.

Owens, D. H., & Hätönen, J. (2005). Iterative learning control - an optimization paradigm. *Annual Reviews In Control*, *29*(1), 57–70.

Paszke, W., Rogers, E., & Gałkowski, K. (2016). Experimentally verified generalized KYP lemma based iterative learning control design. *Control Engineering Practice*, *53*, 57–67.

Press, W. H., Teukolsky, S. A., Vetterling, W. T., & Flannery, B. P. (2007). *Numerical recipes, the art of scientific computing* (3rd ed.). Cambridge University Press.

Roover, D. D., Bosgra, O. H., & Steinbuch, M. (2000). Internal-model-based design of repetitive and iterative learning controllers for linear multivariable systems. *International Journal Of Control*, *73*(10), 914–929.

Savitzky, A., & Golay, M. J. E. (1964). Smoothing and differentiation of data by simplified least squares procedures. *Analytical Chemistry*, *36*(8), 1627–1639.

Sawa, M., & Oohori, J. (1995). Application of thermal spraying technology at steel-works, thermal spraying: Current status and future trends. In *Proceedings of the 14th international thermal spray conference* (pp. 37–42). Kobe, Japan: High Temperature Society of Japan.

Sörnmo, O., Bernhardsson, B., Kröling, O., Gunnarsson, P., & Tenghamn, R. (2016). Frequency-domain iterative learning control of a marine vibrator. *Control Engineering Practice*, *47*, 70–80.

Stadler, G., Steinboeck, A., Baumgart, M., Ettl, A., & Kugi, A. (2019). Model-based estimation of the stress-strain curve of metal strips. *Mathematical And Computer Modelling Of Dynamical Systems*, *25*(3), 224–241.

Stadler, G., Steinboeck, A., & Kugi, A. (2017). Control of curvature and contact force of a metal strip at the strip-roll contact point. *IFAC-PapersOnLine*, *50*(1), 11325–11330.

Steinboeck, A., Baumgart, M., Stadler, G., Saxinger, M., & Kugi, A. (2015). Dynamical models of axially moving rods with tensile and bending stiffness. *IFAC-PapersOnLine*, *48*(1), 598–603.

Steinboeck, A., Mühlberger, G., & Kugi, A. (2014). Control of strip tension in a rolling mill based on loopers and impedance control. *IFAC Proceedings Volumes*, *47*(3), 10646–10651, 19th IFAC World Congress.

Strommer, S., Niederer, M., Steinboeck, A., & Kugi, A. (2014). A mathematical model of a direct-fired continuous strip annealing furnace. *International Journal Of Heat And Mass Transfer*, *69*, 375–389.

Upadhyay, D., & Schaal, C. (2020). Optimizing the driving trajectories for guided ultrasonic wave excitation using iterative learning control. *Mechanical Systems And Signal Processing*, *144*, Article 106876.

Wang, L., Freeman, C. T., & Rogers, E. (2016). Predictive iterative learning control with experimental validation. *Control Engineering Practice*, *53*, 24–34.

Wang, Z., Pannier, C. P., Barton, K., & Hoelzle, D. J. (2018). Application of robust monotonically convergent spatial iterative learning control to microscale additive manufacturing. *Mechatronics*, *56*, 157–165.

Wijdeven, J., & Bosgra, O. (2010). Using basis functions in iterative learning control: analysis and design theory. *International Journal Of Control*, *83*(4), 661–675.

Zhang, S., Zhang, Q., Gu, J., Su, L., Li, K., & Pecht, M. (2021). Visual inspection of steel surface defects based on domain adaptation and adaptive convolutional neural network. *Mechanical Systems And Signal Processing*, *153*, Article 107541.